Quantum Phase Interference and Néel-Vector Tunneling in Antiferromagnetic Molecular Wheels

O. Waldmann,[1,*] T. C. Stamatatos,[2] G. Christou,[2] H. U. Güdel,[3] I. Sheikin,[4] and H. Mutka[5]

[1]*Physikalisches Institut, Universität Freiburg, D-79104 Freiburg, Germany*
[2]*Department of Chemistry, University of Florida, Gainesville, Florida 32611-7200, USA*
[3]*Department of Chemistry and Biochemistry, University of Bern, 3012 Bern, Switzerland*
[4]*Grenoble High Magnetic Field Laboratory, CNRS, BP 166, 38042 Grenoble Cedex 9, France*
[5]*Institut Laue-Langevin, 6 Rue Jules Horowitz, BP 156, F-38042 Grenoble Cedex 9, France*

(Received 15 December 2008; published 13 April 2009)

The antiferromagnetic molecular wheel Fe_{18} of 18 exchange-coupled Fe^{III} ions has been studied by magnetic torque, magnetization, and inelastic neutron scattering. The combined data show that the low-temperature magnetism of Fe_{18} is very accurately described by the Néel-vector tunneling (NVT) scenario, as unfolded by semiclassical theory. In addition, the magnetic torque as a function of applied field exhibits oscillations that reflect the oscillations in the NVT splitting with field due to quantum phase interference.

DOI: 10.1103/PhysRevLett.102.157202 PACS numbers: 75.50.Xx, 33.15.Kr, 71.70.−d, 75.10.Jm

Although magnetism is *a priori* quantum mechanical, observation of genuine quantum phenomena such as tunneling and phase interference in magnets is difficult. This is because in ferro- or ferrimagnets, the low-temperature magnetism and dynamics are by and large well described by the magnetization vector $\mathbf{M}$ obeying classical equations, although for magnetic molecules (e.g., Mn_{12}, Fe_8), tunneling of the magnetization and phase interference have been observed [1]. Antiferromagnets, however, exhibit zero magnetization in the ground state, and observation of quantum behavior is even more challenging.

Antiferromagnets can be described by the Néel vector $\mathbf{n} = (\mathbf{M}_A - \mathbf{M}_B)/(2M_0)$, with sublattice magnetizations $\mathbf{M}_A$, $\mathbf{M}_B$ of length M_0 [Fig. 1(b)]. In three dimensions, they exhibit long-range Néel order, but domains enable thermally activated or even quantum fluctuations of the Néel vector [2]. Nanosized, single-domain antiferromagnetic (AFM) clusters would provide clean systems to study Néel-vector dynamics, but monodispersity is then a key issue. In small particles with weak magnetic anisotropy, the Néel vector can rotate [3,4], while with strong anisotropy it is localized in distinguishable directions, but fluctuates by quantum tunneling, i.e., Néel-vector tunneling (NVT) [5–7]. Typically, there are two tunneling paths [Fig. 1(c)] and interference occurs due to the phase of the wave function. This gives rise to characteristic oscillations in the tunnel splitting as function of applied magnetic field, which would be observable in static measurements such as magnetization [7].

Initial attempts to establish NVT with the ferritin protein [8] unfortunately proved controversial owing to polydisperse samples and the presence of uncompensated magnetization [9]. Recent attempts with the AFM molecular wheels $CsFe_8$ and Fe_{10} were encouraging steps forward [10,11], but were criticized with arguments that the tunneling actions $S_0/\hbar$ are too small and the NVT picture only approximately valid [11]. The latter attempts were stimulated by the theoretical prediction of NVT in such wheels [7], and that its observation would be assisted by the monodispersity and crystallinity inherent in molecular compounds, and their resulting well-defined structural and magnetic parameters [4,12–14].

We here present measurements of the magnetic torque ($\tau = \mathbf{M} \times \mathbf{B}$), magnetization, and inelastic neutron scattering (INS) on the AFM molecular wheel $[Fe_{18}(pd)_{12} - (pdH)_{12}(O_2CEt)_6(NO_3)_6](NO_3)_6$, or Fe_{18} [Fig. 1(a)]. The combined data show that the low-temperature magnetism in Fe_{18} is very accurately described by the NVT scenario, as unfolded by semiclassical theory [7]. Moreover, the torque is found to exhibit wiggles that directly reflect the oscillations in the tunnel splitting with field, or quantum phase interference indeed.

The generic spin Hamiltonian for AFM wheels is

$$\hat{H} = -J\sum_{i=1}^{N}\hat{\mathbf{S}}_i \cdot \hat{\mathbf{S}}_{i+1} + D\sum_{i=1}^{N}\hat{S}_{iz}^2 + g\mu_B\hat{\mathbf{S}} \cdot \mathbf{B}, \qquad (1)$$

with nearest-neighbor Heisenberg interactions of strength $J < 0$ (periodic boundaries assumed), a uniaxial single-ion magnetic anisotropy of strength D along the wheel axis z, and a Zeeman interaction ($N = 18$ is the number of ions, $\hat{\mathbf{S}}_i$ is the spin operator of the ith ion with spin $s = 5/2$ for Fe^{III}). The path-integral treatment—or semiclassical the-

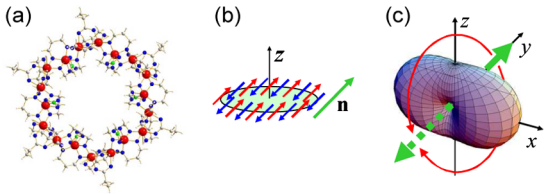

FIG. 1 (color online). (a) Molecular structure of Fe_{18} [red (gray): Fe^{III}]. (b) Schematics of the classical ground-state configuration of the Fe spins (short arrows) and the Néel vector (long arrow, length not to scale). (c) Shape of the potential $V(\mathbf{n})$ in the high-field regime ($g\mu_B B/\hbar\omega_0 = 1.2$). The two tunneling paths from $\mathbf{n} = +y$ to $-y$ are indicated.

ory—of Eq. (1) has provided analytic results for the low-T magnetism and describes its dynamics in terms of the intuitive picture of NVT [7].

For $D > 0$ and a field B along x perpendicular to z, the Néel-vector dynamics are governed by the potential $V(\mathbf{n}) = N/|8J|(g\mu_B B)^2 n_x^2 + Ns^2 D n_z^2$, with hard-axis anisotropies due to the field $\|x$ and the magnetic anisotropy $\|z$. Thus, $V(\mathbf{n})$ has minima at $\mathbf{n} = \pm y$ separated by an energy barrier [Fig. 1(c)]. NVT between these two classical states occurs if the energy barrier is much larger than the attempt frequency $\hbar\omega_0 = s\sqrt{8D|J|}$, producing a tunnel splitting Δ in the quantum-mechanical energy spectrum. In the high-field regime $g\mu_B B > \hbar\omega_0$ the anisotropy barrier is smaller than that due to the field. Hence, the Néel vector tunnels via the z axis, through the anisotropy barrier $U = Ns^2 D$, but the tunneling from, e.g., $+y$ to $-y$ may be either along the "upper" or "lower" path in Fig. 1(c). However, the phase of the wave function acquires a term $\pi/2$ due to quantum fluctuations plus a topological term $\pi N g\mu_B B/|4J|$ proportional to the field. Thus, with increasing field one repeatedly tunes through destructive and constructive interference, and the tunnel splitting oscillates between zero and a maximum according to

$$\Delta(B) = \Delta_0 \left| \sin\left(\pi \frac{N g \mu_B B}{4|J|}\right) \right|, \qquad (2)$$

with $\Delta_0 = 8\hbar\omega_0\sqrt{S_0/h}\exp(-S_0/\hbar)$ and the tunneling action $S_0/\hbar = Ns\sqrt{2D/|J|}$. $S_0/\hbar$ is a crucial parameter: the above condition for NVT to occur translates into $S_0/\hbar > 2$ (henceforth we specify $D/|J|$ in terms of $S_0/\hbar$). Importantly, the tunneling affects also the ground-state energy $\varepsilon_0(B) = \varepsilon(B) - \Delta(B)/2$, where $\varepsilon(B)$ varies smoothly, typically quadratically with B [7]. Hence, the oscillations in $\Delta(B)$ can be detected, at zero temperature, via the static magnetization or torque [7].

Fe_{18} was synthesized as in Ref. [14]. Torque and magnetization data were recorded on single crystals with excellent quality. The shapes were three-sided pyramidal, allowing accurate alignment of the crystals. Torque was measured with a CuBe cantilever inserted into the M10 magnet at the Grenoble High Magnetic Field Laboratory equipped with an Oxford dilution fridge. Magnetic field was in the xz plane, with an angle θ between field and z. Magnetization was measured with the same device, but displaced from the magnet's field center, which resulted in a Faraday force proportional to the magnetization. Despite very careful alignment, a small torque contribution to the signal could not be avoided; hence only the parts of the data are shown where the estimated torque contribution is smaller than 5%. A smooth background is also present, which is estimated to be smaller than 5%. INS spectra of a polycrystalline sample of undeuterated Fe_{18} were recorded on the spectrometer IN5 at the Institut Laue-Langevin, Grenoble. Data were corrected for detector efficiency by a vanadium standard. The initial wavelength was $\lambda = 5.0$ Å and the temperatures were $T = 1.5$ and 4.2 K. Spectra were summed over all detector banks. Experimental resolution at the elastic line was 95 μeV.

The magnetization and torque curves vs field at $T = 0.1$ K are shown in Figs. 2(a) and 2(c) for fields (nearly) parallel to z. Both curves exhibit staircaselike steps at regular field intervals, as is common in AFM wheels [4,12,15]. However, for fields perpendicular to z, the magnetization, after a first broad step, increases linearly with field, with only weak features apparent [Fig. 2(b)]. The torque is even more striking: after a first step it exhibits wiggles at higher fields [Fig. 3(a)]—this is unprecedented for spin clusters in general, and AFM wheels in particular [16]. The wiggles in the torque directly correspond to oscillations in the NVT splitting (*vide infra*), and their observation is the main result of this work.

The sign of the torque [Figs. 2(c) and 3(a)] determines $D > 0$. As pointed out in Ref. [7], the semiclassical theory then predicts a dichotomy in the magnetization as a key feature of NVT, i.e., a conventional staircaselike behavior for parallel fields but a linear curve with weak features for perpendicular fields—exactly as observed in Fe_{18}. This is a first, strong indication of the accuracy of the NVT picture in Fe_{18}. The field derivative of the parallel magnetization [Fig. 4(a)] and the positions of the maxima (steps in the magnetization) shown in Fig. 4(b) demonstrate the regular field intervals of the steps. The dependence of the first torque step on the field angle, $B_1(\theta)$, is presented in Fig. 4(c) (features at higher fields show similar dependencies, but with much weaker variation). In AFM wheels studied before, the angle dependence is well described by $B_1(\theta) = a + b(\cos^2\theta - 1/3)$, which was also observed for the wheels $CsFe_8$ and Fe_{10} with the largest $S_0/\hbar$ reported to date [10,17]. Fe_{18} shows a more pronounced angle dependence indicating a substantially larger $S_0/\hbar$. Figure 4(d) presents the INS spectra at 1.5 and 4.2 K. Four transitions I, II, iii, and iv at ca. 0.3, 1.0, 0.8, and 1.35 meV, and a weak feature v at ca. 0.6 meV are observed for positive energy

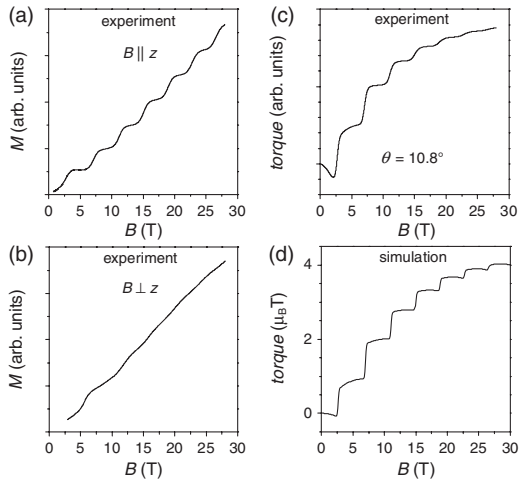

FIG. 2. Magnetization vs field for (a) $B \parallel z$ and (b) $B \perp z$, and torque vs field for B nearly parallel to z as (c) measured and (d) simulated using Eq. (3) ($T = 0.1$ K).

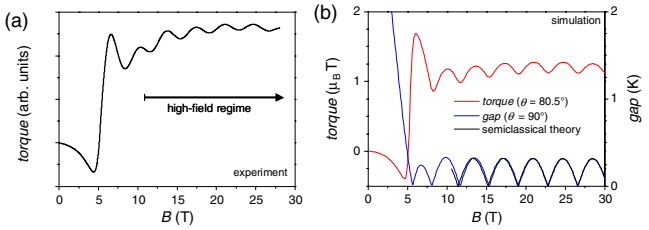

FIG. 3 (color online). Torque vs field for B nearly perpendicular to z as (a) measured and (b) simulated ($\theta = 80.5°$, $T = 0.1$ K). Panel (b) also shows the gap between the two lowest quantum states vs B as simulated with Eq. (3) [blue (dark gray) curve] and predicted by semiclassics, Eq. (2) (black curve).

transfer. At negative energy transfer, the expected anti-Stokes lines I' and iv' are visible. From the temperature dependence, peaks I and II are cold transitions, and iii, iv, and v are hot transitions.

The combined data establish an AFM wheel, and Eq. (1) with a large $S_0/\hbar$. The molecular structure of Fe_{18} means that not all exchange paths are identical, as assumed in Eq. (1). However, the energies of the low-lying states relevant in our experiments are not affected, to first order, by variations in the exchange constants [18]. J should thus be taken as the average, as is also the case for the anisotropy constant D. Thus, with a modulation in the exchange and anisotropy parameters, Eq. (1) is the appropriate model to describe the low-T behavior of Fe_{18} (and therewith also the models discussed next).

Since the Hilbert space for Fe_{18} is huge ($\approx 10^{14}$), preventing direct use of Eq. (1), our quantitative analysis employs two approximations, which capture the low-energy, i.e., low-T physics well. First, the AFM sublattices

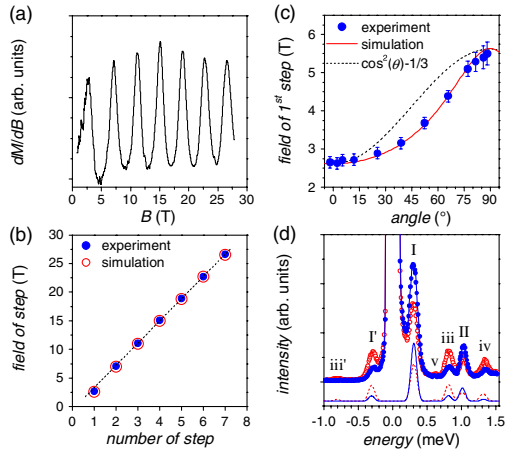

FIG. 4 (color online). (a) dM/dB vs field for $B \parallel z$ ($T = 0.1$ K). (b) Fields of the maxima in dM/dB as measured (solid circles) and simulated (open circles). (c) Field of the first torque step vs angle, $B_1(\theta)$, as observed (circles), expected in the strong-exchange limit (dashed line), and simulated with Eq. (3) (solid line). (d) INS spectra at 1.9 (solid circles) and 4.2 K (open circles). Solid and dashed lines show the simulated spectra (elastic line not included in simulation).

are replaced by spins $\hat{\mathbf{S}}_A = \sum_{i\in A}\hat{\mathbf{S}}_i$ and $\hat{\mathbf{S}}_B = \sum_{i\in B}\hat{\mathbf{S}}_i$, each of length $Ns/2 = 45/2$. This gives

$$\hat{H}_{AB} = -j\hat{\mathbf{S}}_A \cdot \hat{\mathbf{S}}_B + d(\hat{S}^2_{Az} + \hat{S}^2_{Bz}) + g\mu_B\hat{\mathbf{S}} \cdot \mathbf{B}, \quad (3)$$

with $j = a_1 J$ and $d = b_1 D$ [18]. The Hilbert space of Eq. (3) is small (2116), which permits exact numerical diagonalization. Second, we will use the analytical results of the semiclassical treatment of Eq. (1) [7].

Diagonalizing Eq. (3) and fitting to the data of Figs. 4(b)–4(d) gave $j = -5.1(1)$ K, $d = 0.021(1)$ K ($g = 2.0$). This parameter set reproduces all our data with high accuracy ($\pm$ a few percent), i.e., the fields of the magnetization steps [Fig. 4(b)], the angle dependence $B_1(\theta)$ [Fig. 4(c)], the INS spectra [Fig. 4(d)], and the torque curves for nearly parallel [Figs. 2(c) and 2(d)] and perpendicular fields (Fig. 3). Hence, Eq. (3), and therewith Eq. (1), describes the low-energy sector of Fe_{18} very accurately. The observed features in the torque (and magnetization) are less sharp than in the simulations (Fig. 3), and possible reasons for this include (i) additional, very weak terms in the spin Hamiltonian, e.g., Dzyaloshinski-Moriya interactions, which would lead to a rounding of the gap function and hence the torque, and (ii) a small distribution (5%) in the j and d values (j and d strain), which would result in a distribution of step positions and hence broadening.

Determining J and D now requires knowing a_1, b_1. In principle, a_1 and b_1 should be determined such that the exact low-energy spectra of Eqs. (1) and (3) match [18]. This is not trivial for Fe_{18}. Quantum Monte Carlo techniques yielded $a_1 = 0.2721$ [19], and extrapolating b_1 for $N = 6$, 8, 10 to Fe_{18} [18] yields the estimate $b_1 \approx 0.07$. Hence, $J = -19$ K and $D \approx 0.3$ K, which are typical values for ferric wheels. With these one gets $S_0/\hbar = 8.0$.

We now turn to semiclassical theory. First a subtle point needs to be addressed. The above method of determining a_1, b_1 is certainly correct, but we observe that semiclassical theory yields quantitatively accurate results only if one uses the a_1, b_1 values predicted by itself. This is expected from self-consistency considerations. Hence, semiclassical formulas should be used with "corrected" J, D values as deduced with the semiclassical values $a_1^{sc} = 2/9$, $b_1^{sc} = 0.1065$ [20]. The tunneling action then becomes $S_0/\hbar = 5.90$, which is the value to be used [21].

Henceforth we consider the high-field regime $g\mu_B B > \hbar\omega_0$, or $B > 10.6$ T for Fe_{18}. The criterion for NVT is $S_0/\hbar > 2$, which is well fulfilled by $S_0/\hbar = 5.90$. The expectation value of the Néel vector along $\pm y$ is $\langle 0|n_y|0\rangle^2 \approx 1 - (S_0/\hbar)^{-1}$ [7], hence in Fe_{18} the Néel vector is localized to 83%. Another figure of merit is the ratio Δ_0/U of maximal tunnel splitting vs barrier height. For Fe_{18}, $\Delta_0 = 0.320$ K and $U = 22.2$ K, thus $\Delta_0/U = 0.014$; the tunnel splitting is exponentially small as expected for a tunneling scenario. Figure 3(b) displays the energy gap between the two lowest levels for perpendicular fields as calculated with Eq. (3) and the semiclassical

formula Eq. (2). The excellent quantitative agreement finally demonstrates the high accuracy of the semiclassical NVT theory for Fe_{18}.

With reliable values for j, d, $S_0/\hbar$, and the accuracy of our modeling of Fe_{18} established, we now discuss the wiggles in the torque for nearly perpendicular fields. Figure 3(b) shows the calculated field dependencies for the energy gap and the torque. In the high-field regime, the energy gap (= tunnel splitting) exhibits the typical sinus-half-wave oscillation due to quantum interference [7]. Comparison with the torque is striking: in the high-field regime the torque clearly follows the tunnel splitting, except for a smooth offset. The torque has not yet been calculated by semiclassical theory, but the result for M_x [7] inspires a refinement, which we checked numerically to describe the torque. For $\theta \approx 90°$, we write the magnetization as $\mathbf{M} = g\mu_B B(F_x, 0, \cos\theta F_z)$ and the torque as $\tau = g\mu_B B \cos\theta(F_z - F_x)$, where, at 0 K,

$$F_{x/z} = \frac{B}{B_0} - \frac{1}{2} + \frac{\pi N \Delta_0}{8|J|}(-1)^n \cos\left(\pi \frac{B}{B_0} \pm \phi_{x/z}\right) \mp f_{x/z}. \tag{4}$$

Here we used $B_0 = 4|J|/(Ng\mu_B)$ and a factor $(-1)^n$ such that $|\sin(\cdots)| = (-1)^n \sin(\cdots)$ (n numbers magnetization or torque steps). As compared to the semiclassical formula for M_x we have, to grasp weak but important effects of magnetic anisotropy, introduced shifts $\phi_x(B)$, $\phi_z(B)$ to take into account that the steps do not occur exactly at fields nB_0, and functions $f_x(B)$, $f_z(B)$ to account for a smooth offset. Numerically we find that ϕ_x, ϕ_z, f_x, and f_z vary with field roughly as B^{-1}, in accord with expectation, such that after some rearrangements

$$\tau = \frac{\pi N}{4|J|}\Delta_0 \left|\sin\left(\pi \frac{B}{B_0}\right)\right| g(B)\cos\theta + f(B), \tag{5}$$

where $g(B)$ and $f(B)$ are smooth, essentially constant functions of B. The torque provides only indirect evidence for the size of the NVT splitting, but Eq. (5) proves that it does directly probe the oscillations in the NVT splitting, as demonstrated before in Fig. 3(b). At nonzero temperatures, the sine term in Eq. (5) should be multiplied by $\tanh(\Delta/2k_BT)$, which has the effect of smearing out sharp features, or of rounding the torque wiggles. This is why the simulated torque curve in Fig. 3(b) is less sharp at the zeros than the gap.

In summary, the combined magnetic torque, magnetization, and INS data, and their analyzes by two models, demonstrate that the low-temperature magnetism in Fe_{18} is in accord with the NVT picture of semiclassical theory. Most importantly, the observed features in the magnetic torque have been demonstrated to directly reflect oscillations in the NVT splitting, i.e., quantum phase interference. An interesting point is the number of electrons involved in the tunneling. In Fe_{18}, the total spin on each AFM sublattice has a length of $45/2$, i.e., 90 electrons are involved. Hence, the disconnectivity, which is a measure for the "macroscopiness" of a quantum effect [22], is 90. This makes Fe_{18} one of the most mesoscopic molecular systems exhibiting magnetic quantum tunneling.

Financial support by the Deutsche Forschungsgemeinschaft (DFG) and the U.S. National Science Foundation (CHE-0414555) are acknowledged.

*oliver.waldmann@physik.uni-freiburg.de

[1] D. Gatteschi, R. Sessoli, and J. Villain, *Molecular Nanomagnets* (Oxford University Press, Oxford, U.K., 2006); J. R. Friedman *et al.*, Phys. Rev. Lett. **76**, 3830 (1996); W. Wernsdorfer and R. Sessoli, Science **284**, 133 (1999).
[2] O. G. Shpyrko *et al.*, Nature (London) **447**, 68 (2007).
[3] P. W. Anderson, *Basic Notions of Condensed Matter Physics* (Benjamin/Cummings Publishing Co., Menlo Park, CA, 1984).
[4] O. Waldmann, Coord. Chem. Rev. **249**, 2550 (2005).
[5] E. M. Chudnovsky and J. Tejada, *Macroscopic Quantum Tunneling of the Magnetic Moment* (Cambridge University Press, Cambridge, U.K., 1998).
[6] B. Barbara and E. Chudnovsky, Phys. Lett. A **145**, 205 (1990).
[7] A. Chiolero and D. Loss, Phys. Rev. Lett. **80**, 169 (1998).
[8] S. Gider *et al.*, Science **268**, 77 (1995); J. Tejada *et al.*, Phys. Rev. Lett. **79**, 1754 (1997).
[9] J. Tejada, Science **272**, 424 (1996); A. Garg, *ibid.* **272**, 424 (1996); S. Gider *et al.*, *ibid.* **272**, 425 (1996).
[10] O. Waldmann *et al.*, Phys. Rev. Lett. **95**, 057202 (2005).
[11] P. Santini *et al.*, Phys. Rev. B **71**, 184405 (2005).
[12] K. L. Taft *et al.*, J. Am. Chem. Soc. **116**, 823 (1994).
[13] D. Gatteschi *et al.*, Science **265**, 1054 (1994).
[14] P. King, T. C. Stamatatos, K. A. Abboud, and G. Christou, Angew. Chem., Int. Ed. Engl. **45**, 7379 (2006).
[15] A. Cornia *et al.*, Angew. Chem., Int. Ed. Engl. **38**, 2264 (1999).
[16] "Wiggles" in the torque vs field were observed before in $Mn-[3\times 3]$, Cr_7Ni, and Cr_7Zn, but these are not due to NVT but a direct, first-order mixing of $|S,-S\rangle$ and $|S+1,-S-1\rangle$ levels by the magnetic anisotropy [O. Waldmann *et al.*, Phys. Rev. Lett. **92**, 096403 (2004) and [17]]. Experimentally, this situation is unambiguously distinguished from the observations in Fe_{18} by the fact that the wiggles occur for both nearly parallel and perpendicular fields, in striking contrast to Fe_{18}, where ordinary staircaselike profiles are observed for parallel fields. The situation in Fe_{18} hence cannot be confused with that found in the above molecules. It is noted that in high fields NVT cannot be described by a mixing of $|S,-S\rangle$ and $|S+1,-S-1\rangle$ states.
[17] S. Carretta *et al.*, Phys. Rev. B **72**, 060403(R) (2005).
[18] O. Waldmann, Europhys. Lett. **60**, 302 (2002).
[19] L. Engelhardt and M. Luban, Phys. Rev. B **73**, 054430 (2006).
[20] $a_1^{sc} = 4/N$, $b_1^{sc} = 2Ns^2/[Ns(Ns+2)-3]$ [7,18].
[21] Unfortunately, this point was not considered before, and previously reported $S_0/\hbar$ values should be used with care.
[22] A. J. Leggett, J. Phys. Condens. Matter **14**, R415 (2002).